MODELING PHOTOVOLTAIC GRID INTER-SHADING

by

Biljana CHITKUSHEVA DIMITROVSKA[a*], Marko CEPIN[b], Roman GOLUBOVSKI[c], and Hristina SPASEVSKA[d]

[a] Faculty of Electrical Engineering, University Goce Delcev, Stip, N. Macedonia
[b] Faculty of Electrical Engineering, University of Ljubljana, Ljubljana, Slovenia
[c] Faculty of Natural Sciences and Mathematics, Ss. Cyril and Methodious, Skopje, N. Macedonia
[d] Faculty of Electrical Engineering and Information Technologies, Ss. Cyril and Methodious, Skopje, N. Macedonia

Original scientific paper
https://doi.org/10.2298/TSCI200116169C

Photovoltaic energy conversion is an efficient renewable source affordable as a technology even on the household level. Several technological aspects are subject to continuous improvement. This paper tackles the possibilities for denser panel population of a photovoltaic plant thus more efficient space utilization. The objective is to develop a mathematical model of inter-shading among the photovoltaic panels. The model calculates the electrical energy obtained from panels and considers the shading among the panels. The geographical location of the plant location, the distances between the solar panels and their angle of inclination, the dimensions of the panels and the time interval under evaluation are the parameters which are important for placing the power plant. The results show how much electric energy can be obtained from a certain set of photovoltaic panels. The results indicate, what are the distances between the panels for better allocation of resources when deciding on the number of solar panels and their arrangement.

Key words: *inter-shading, photovoltaic grid, solar energy production, renewable energy*

Introduction

Renewable energy technologies produce energy by converting natural phenomena into useful forms of energy [1-4]. Photovoltaic (PV) cells are devices that use semiconductor materials to convert the sunlight into electrical energy.

The PV manufacturers provide warranties for PV panels in terms of both life expectancy and efficiency. Generally, the PV panels can last up to 25 years or more with an efficiency loss of 18% during 20 years of operation [5]. As compared to wind turbines, PV panels operate without any noise or moving parts. The PV panels require low maintenance, their operating costs are minimal, and they are highly suitable for remote applications. A grid-connected PV system consists of solar panels, one or several inverters, a power conditioning unit and grid connection equipment. Several researchers have dealt with this issue [1-8]. Their research is based on the optimal placement of solar panels depending on the angle of inclination. So, they have been analyzing just one parameter and how that parameter affected the output energy. Taking one parameter and its effect on the energy production is one of the limitations of previous re-

* Corresponding author, e-mail: biljana.citkuseva@ugd.edu.mk

search. Multiple parameters such as: the angle of inclination, the geographical location, and the distances between the solar panels (distances between the rows and columns) are extremely important in designing a photovoltaic plant. These are the variables with the biggest influence on the generation on energy. Each of them must be analyzed separately and the parameter with the greatest impact must be determined.

The objective of this paper is to elaborate a theoretical model for the inter-shading of PV power plant consisting of 9 PV panels placed in three rows and three columns. The goal is to determine analytically the inter-shading during the day and the year and consequently how the shading affects energy production [6, 7].

Solar angles

The basic parameter for determining inter-shading among the panels in a dense PV grid is the sun incidence angle, θ. The incidence angle, θ, is the angle formed by the Sun rays and the perpendicular line at a particular geolocation. Incidence angle, θ, (shown in fig. 1, [5]) is related to the other solar angles. The general expression for the angle of incidence is:

$$\begin{aligned}\cos\theta = \sin\delta\sin L\cos\beta - \sin\delta\cos L\sin\beta\cos z_s + \cos\delta\cos L\cos\beta\cos h + \\ + \cos\delta\sin L\sin\beta\cos z_s\cos h + \cos\delta\sin\beta\sin z_s\sin h\end{aligned} \tag{1}$$

where δ is declination angle, β – the surface tilt angle, L – the local latitude, h – the hour angle, and z_s – the surface azimuth angle.

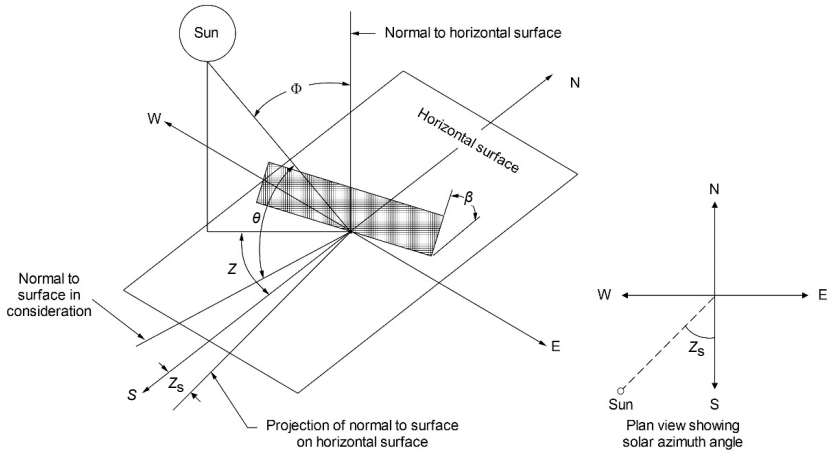

Figure 1. Solar angles

Determining this angle requires modeling of solar irradiation geometry for specific geolocation. Incidence angle for specific geolocation requires determination of solar altitude angle, α, and solar azimuth angle, z, at specific moment. This specific moment is determined by date and time. The altitude angle, α, and the azimuth angle, z, are two fundamental parameters for determination of the exact position of the Sun with respect to specific geolocation at any time in the day and they are used for solar design projects. The solar altitude angle is the angle between the sun rays and the equatorial plane, and it oscillates through the year being higher in summer and lower in winter. The mathematical expression for the solar altitude angle is eq. (2), [5] the following.

$$\sin(\alpha) = \cos(\Phi) = \sin(L)\sin(\delta) + \cos(L)\cos(\delta)\cos(h) \tag{2}$$

where L is the local latitude. Northern hemisphere latitudes are positive, and southern hemisphere latitudes are negative. The altitude angle depends on three fundamentals angles: the solar declination, δ, the latitude, L, and the solar hour angle, h, fig. 2, [5, 8, 9]. Equations that define these solar angles are given. Declination, δ, can be calculated approximately for any day in a year, n, with the eq. (3), [5]:

$$\delta = 23,45 \sin\left[\frac{360}{365}(284+n)\right] \tag{3}$$

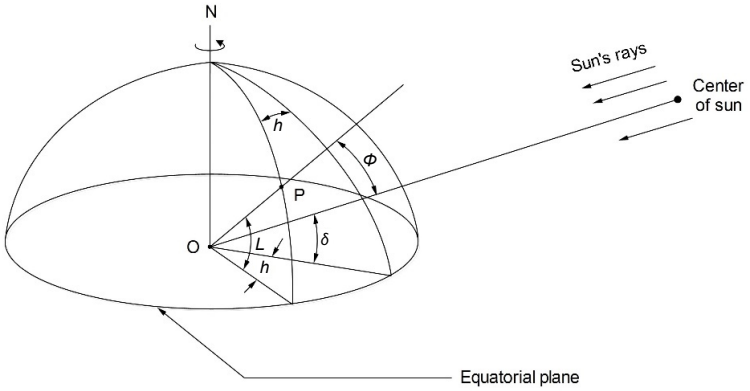

Figure 2. Definition of latitude, hour angle and solar declination

The declination ranges from 0° at the spring equinox to 23.45° at the summer solstice, 0° at the fall equinox to –23.45° at the winter solstice. The solar declination angle varies slowly and can be considered constant for a specific day, eq. (3).

The solar hour angle, h, of a point on the earth's surface is defined as the angle through which the earth would turn to bring the meridian of the point directly under the Sun. The equation [5] for hour angle is:

$$h = (AST - 12)15 \tag{4}$$

The solar angle depends on the apparent solar time (AST). In solar irradiation geometry calculations, AST must be used to express the time of day. To convert the local standard time (LST) to apparent solar time two corrections are applied: the equation of time and the longitude correction. The corrections are implemented by the following equations [5]:

$$AST = LST + ET \pm 4(SL - LL) - DS \tag{5}$$

$$ET = 9.87\sin(2B) - 7.53\cos(B) - 1.5\sin(B) \ \ [\text{min}] \tag{6}$$

$$B = (n-81)\frac{360}{364} \tag{7}$$

where LST is local standard time, ET – the equation of time, SL – the standard longitude, LL – the local longitude, and DS – the daylight saving (0 or 60 min).

The solar azimuth angle, z, is the angle of the sun's rays measured in the equatorial plane from the due south (true south) for the northern hemisphere or due north for the southern hemisphere and it represents daylight as shown on fig. 1. The solar azimuth angle depends on three fundamentals angles: the solar declination, δ, the altitude angle, α, and the solar hour

angle, h. The equations for these angles are previously given. The mathematical expression for the solar azimuth (z), [5] is:

$$\sin(z) = \frac{\cos(\delta)\sin(h)}{\sin(\alpha)} \tag{8}$$

The equation is correct if:

$$\cos h > \frac{\tan\delta}{\tan L} \tag{9}$$

If not, it means that the Sun is behind the E-W line. Solar azimuth angle for the morning hours is $-\pi+|z|$, and for the afternoon hours is $\pi - z$. The solar altitude and solar azimuth are sufficient to calculate shadow direction and longevity for any geolocation and moment in a day.

Model of PV grid inter-shading

This paper employs a theoretical approach on a mathematical model for shadow determination, including shading geometry and implementation in visual basic application (VBA) in Microsoft Excel. The PV grid taken for the analytical model is 3 × 3.

Inter-shading in a dense PV grid is unavoidable and needs to be minimized. Shadow length changes from infinity at sunset and sunrise to a minimum at noontime [10-13]. Moreover, the shadow length is tallest in winter for the northern hemisphere.

On the flat field, the solar panels are fixed in horizontal level, arranged in three rows distanced by r_y and three columns distanced by r_x. The PV panels have a tilt angle of β, width P_x and length P_y, fig. 3. If the thickness of the panel is ignored, then the shadow that falls on a particular PV panel is a rectangular surface. Proposed shadow model includes a procedure for calculation of the shadow that falls on a particular PV panel within precisely defined 3 × 3 PV grid. Figure 4 shows a typical shade geometry from one panel to another between adjacent rows. The shadow is calculated according to the projections in two axis – in width (X) and length (Y). The dimensions of the shadow on the panel are P_{sh_x} and P_{sh_y}, respectively.

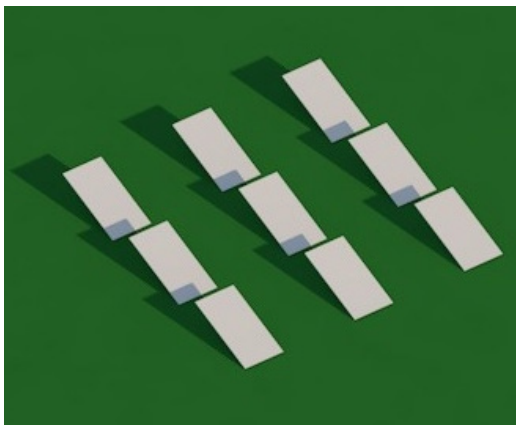

Figure 3. The PV grid 3 × 3 (inter-shading in a winter afternoon)

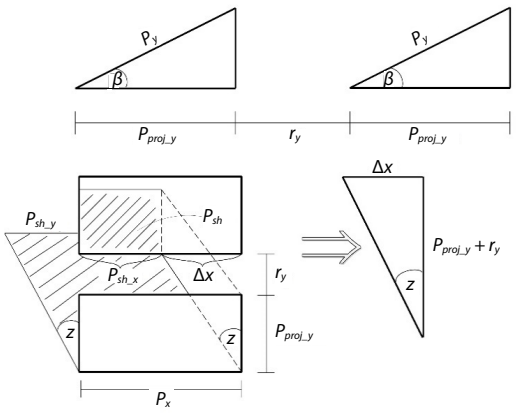

Figure 4. Elements of inter-shading

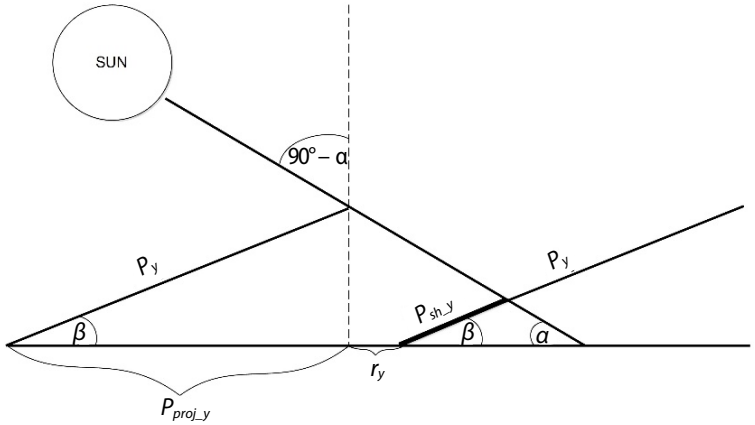

Figure 5. Determination of P_{sh_y}

The P_{sh_y} defines the overlapping shadow in length between rows, fig. 5:

$$P_{sh\_y} = \begin{cases} 0, & P_{sh\_y} < 0 \\ \dfrac{P_y \cot\alpha \sin\beta - r_y}{\cos\beta + \cot\alpha \sin\beta}, & 0 < P_{sh\_y} < P_y \\ P_y, & P_{sh\_y} > P_y \end{cases} \tag{10}$$

If $P_{sh\_y} < 0$ there is no inter-shading. The model defines two configurations:

– $P_x \le r_x$, the horizontal inter-panel gap is greater than or equal to the panel width
– $P_x > r_x$, the gap is less than the width of the panels

In case of no east-west panel inclination, and parallel Sun rays, the panel shadow width can be approximated to P_x. The horizontal shadow overlap P_{sh_x} is calculated according to the specific configuration and based on the azimuth displacement Δx, which is always considered in its absolute value since pre- and after-noon values of the azimuth are symmetrical, ranging between –90° and +90° (the theoretical daylight limits). Where azimuth displacement Δx can be calculated according to fig. 4:

$$P_{proj\_y} = P_y \cos\beta \tag{11}$$

$$\Delta x = (P_{proj\_y} + r_y)\Delta\tan(z) \tag{12}$$

$$z = z_{\text{Sun}} - z_s \tag{13}$$

The z_{Sun} is solar azimuth angle and z_s is surface azimuth angle of orientation. The effective shaded panel surface is:

$$P_{sh} = P_{sh\_x} P_{sh\_y} \tag{14}$$

In the first configuration the panel shadow falls either on a single panel behind or between panels as depicted in fig. 6.

Simulation of both types of situations is depicted in fig. 7. The corresponding situations for the shadow movement Δx are:

– *Case 1:* $0 \le \Delta x < P_x$

Each panel shades the one behind itself in the same column. Shadows are single. Their number is 6, fig 7(a). The total grid surface under shadow can be calculated by:

$$P_{sh} = 6P_{sh\_x}P_{sh\_y} = 6[(P_x - \Delta x)P_{sh\_y}] \tag{15}$$

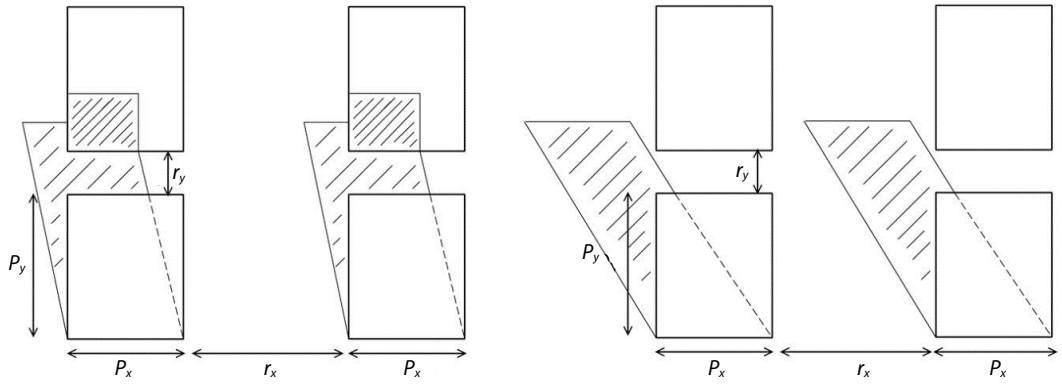

Figure 6. Expected shading in Configuration 1

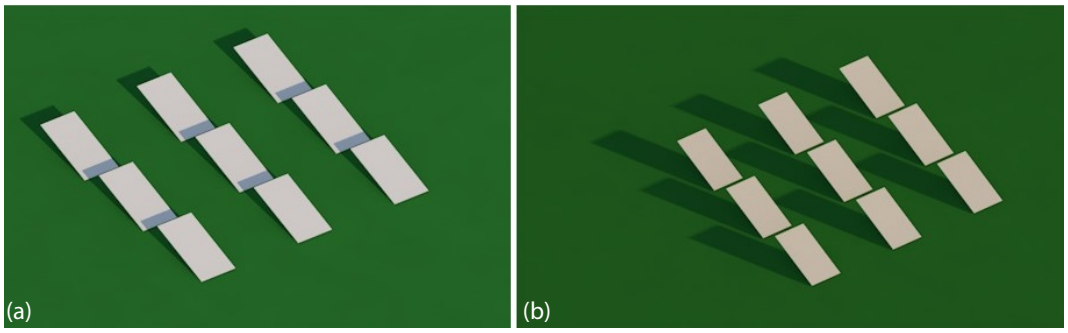

Figure 7. Configuration $P_x \leq r_x$ – Simulation of both types of shadows around noon

– *Case 2*: $P_x \leq \Delta x < r_x$
Shadows fall between the panels, so no grid surface is under shadow, fig 7(b).

$$P_{sh} = 0 \tag{16}$$

– *Case 3:* $r_x \leq \Delta x < P_x + r_x$
Shadows fall behind on the neighboring columns. There are four single shadows on four panels. The shadow surface is:

$$P_{sh} = 4P_{sh\_x}P_{sh\_y} = 4[(\Delta x - r_x)P_{sh\_y}] \tag{17}$$

– *Case 4:* $P_x + r_x \leq \Delta x < 2\Delta P_x + r_x$
Shadows still fall on the four solar panels behind in the neighboring columns, so:

$$P_{sh} = 4P_{sh\_x}P_{sh\_y} = 4[(2P_x + r_x - \Delta x)P_{sh\_y}] \tag{18}$$

– *Case 5:* $2P_x + r_x \leq \Delta x < P_x + 2r_x$
Shadows fall between the panels, so no grid surface is under shadow.

$$P_{sh} = 0 \tag{19}$$

– *Case 6:* $P_x + 2r_x \le \Delta x < 2P_x + 2r_x$

Shadow fall behind over the neighboring column. Under single shadows are two panels of the outmost column. The shadow surface is:

$$P_{sh} = 2P_{sh\_x}P_{sh\_y} = 2[(\Delta x - P_x - 2r_x)P_{sh\_y}] \tag{20}$$

– *Case 7:* $2P_x + 2r_x \le \Delta x < 3P_x + 2r_x$

Shadows still fall on the two panels of the outmost column. The shadow surface is:

$$P_{sh} = 2P_{sh\_x}P_{sh\_y} = 2[(3P_x + 2r_x - \Delta x)P_{sh\_y}] \tag{21}$$

– *Case 8:* $\Delta x \ge 3P_x + 2r_x$

Shadows fall out of the grid, so the surface under the shadow is zero.

$$P_{sh} = 0 \tag{22}$$

Visualizations of configuration 1 using simulation CAD software is given in fig. 7.

In the second configuration, the panel shadow falls behind, either on a single panel or on two panels in two neighboring columns as depicted in fig. 8. Visualizations of both types of situations are depicted in fig. 9. The corresponding situations for the shadow movement Δx in the second configuration are:

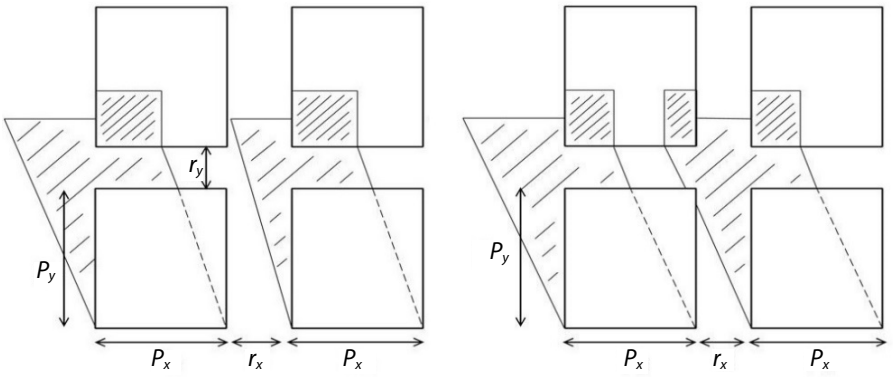

Figure 8. Expected shading in Configuration 2

– *Case 1:* $0 \le \Delta x < r_x$

Each panel shades the one behind itself in the same column. Shadows are single. Their number is 6. The total grid surface under shadow can be calculated with:

$$P_{sh} = 6P_{sh\_x}P_{sh\_y} = 6[(P_x - \Delta x)P_{sh\_y}] \tag{23}$$

– *Case 2:* $r_x \le \Delta x < P_x$

Shadows fall behind on the own and neighboring column. Their number is 6, fig. 9(b). Four of them are double and two are single shadows. The surface under shadow is given by:

$$P_{sh} = 4[(P_x - r_x)P_{sh\_y}] + 2[(P_x - \Delta x)P_{sh\_y}] \tag{24}$$

– *Case 3:* $P_x \le \Delta x < P_x + r_x$

Shadows fall behind on the neighboring columns. Shadows are single. The number of total shadows is 4. The shaded surface is:

$$P_{sh} = 4[(\Delta x - r_x)P_{sh\_y}] \tag{25}$$

– *Case 4:* $P_x + r_x \le \Delta x < P_x + 2r_x$

Shadows fall behind on the own and neighboring column. There are four single shadows, fig. 9(a). The shaded surface is:

$$P_{sh} = 4[(2P_x + r_x - \Delta x)P_{sh\_y}] \tag{26}$$

– *Case 5:* $P_x + 2r_x \le \Delta x < 2P_x + r_x$

Shadows fall behind on the neighboring columns. Two shadows are single and two of them are double. The total shadow surface is:

$$P_{sh} = 2[(P_x - r_x)P_{sh\_y}] + 2[(2P_x + r_x - \Delta x)P_{sh\_y}] \tag{27}$$

– *Case 6:* $2P_x + r_x \le \Delta x < 2P_x + 2r_x$

Each panel shadow falls on the panel over two columns. The shadows are single. Their number are 2. The shaded surface is:

$$P_{sh} = 2[(\Delta x - P_x - 2r_x)P_{sh\_y}] \tag{28}$$

– *Case 7:* $2P_x + 2r_x \le \Delta x < 2P_x + 3r_x$

Shadow fall behind over the neighboring column. Under single shadows are two panels of the outmost column. The shadow surface is:

$$P_{sh} = 2[(3P_x + 2r_x - \Delta x)P_{sh\_y}] \tag{29}$$

– *Case 8:* $2P_x + 3r_x \le \Delta x < 3P_x + 2r_x$

Shadows still fall on the two panels of the outmost column. The shadow surface is:

$$P_{sh} = 2[(3P_x + 2r_x - \Delta x)P_{sh\_y}] \tag{30}$$

– *Case 9:* $\Delta x \ge 3P_x + 2r_x$

Shadows fall out of the grid, so the surface under the shadow is zero.

$$P_{sh} = 0 \tag{31}$$

Visualizations of configuration 2 using simulation CAD software is given in fig. 9.

The algorithm for determining the number of shaded surfaces of the solar panels is given with the flowchart in fig. 10. This model can be extended and algorithmically solved for

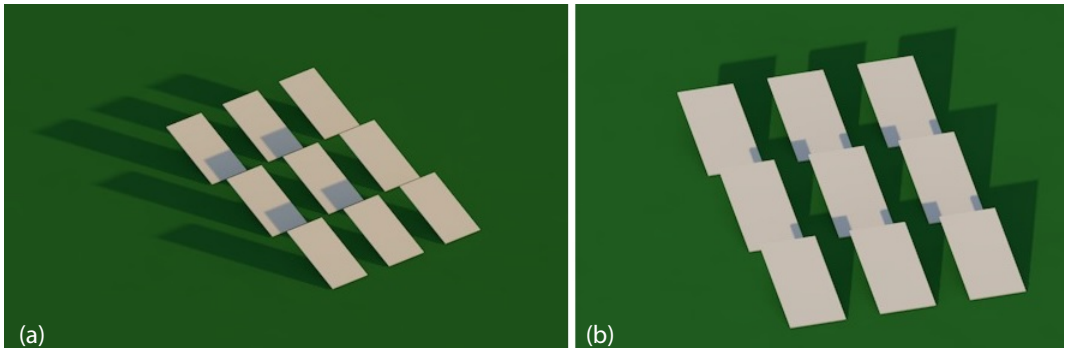

Figure 9. Configuration $P_x > r_x$ – simulation of both types of shadows around noon

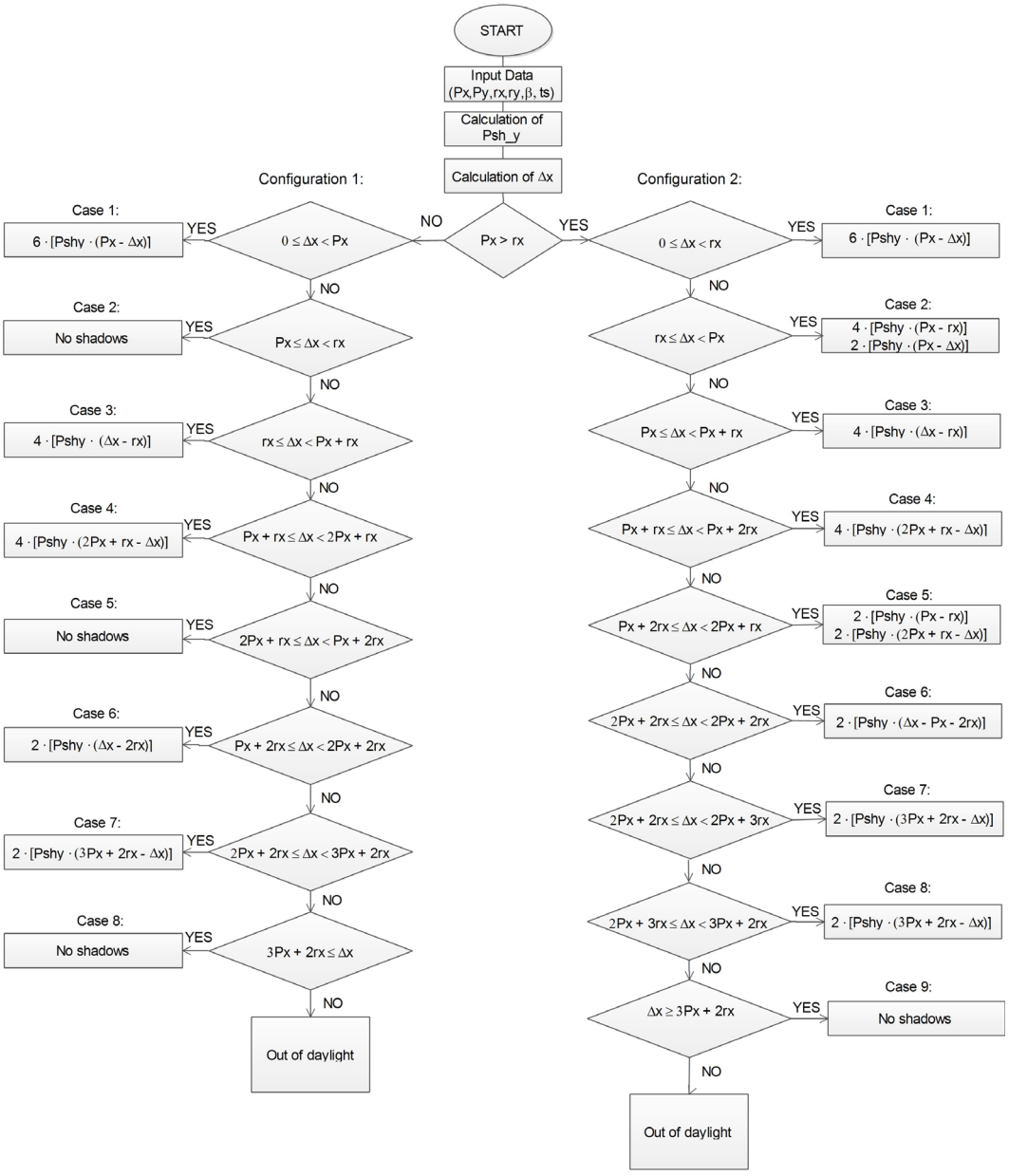

Figure 10. Flowchart for shadow determination

a PV grid of M × N solar panels. The resulting model equation for the surface under the shadow S_{dif} is given with eqs. (32) and (33) for Configurations 1 and 2, respectively. For Configuration 1 ($P_x \le r_x$) :

$$S_{\text{dif}} = P_{sh} = \begin{Bmatrix} 6[(P_x - \Delta x)P_{sh\_y}], & \text{case 1} \\ 0, & \text{case 2} \\ 4[(\Delta x - r_x)P_{sh\_y}], & \text{case 3} \\ 4[(2P_x + r_x - \Delta x)P_{sh\_y}], & \text{case 4} \\ 0, & \text{case 5} \\ 2[(\Delta x - P_x - 2r_x)P_{sh\_y}], & \text{case 6} \\ 2[(3P_x + 2r_x - \Delta x)P_{sh\_y}], & \text{case 7} \\ 0, & \text{case 8} \end{Bmatrix} \tag{32}$$

For configuration 2 $(P_x > r_x)$:

$$S_{\text{dif}} = P_{sh} = \begin{Bmatrix} 6[(P_x - \Delta x)P_{sh\_y}], & \text{case 1} \\ 4[(P_x - r_x)P_{sh\_y}] + 2[(P_x - \Delta x)P_{sh\_y}], & \text{case 2} \\ 4[(\Delta x - r_x)P_{sh\_y}], & \text{case 3} \\ 4[(2P_x + r_x - \Delta x)P_{sh\_y}], & \text{case 4} \\ 2[(P_x - r_x)P_{sh\_y}] + 2[(2P_x + r_x - \Delta x)P_{sh\_y}], & \text{case 5} \\ 2[(\Delta x - P_x - 2r_x)P_{sh\_y}], & \text{case 6} \\ 2[(3P_x + 2r_x - \Delta x)P_{sh\_y}], & \text{case 7} \\ 2[(3P_x + 2r_x - \Delta x)P_{sh\_y}], & \text{case 8} \\ 0, & \text{case 9} \end{Bmatrix} \tag{33}$$

Results

After calculation of the solar parameters, the shadow geometry and consequently the exposed and shaded surfaces, the power output of the entire power plant can be calculated for every moment in time with the following equation:

$$P_{el_5} = G_b S_{\text{dir}} + GdS_{\text{dif}} \tag{34}$$

where G_b is the direct solar radiation, G_d – the diffuse solar radiation, S_{dir} – the surface of the panel exposed to direct radiation, and S_{dif} – the surface of the panel under shadow.

The proposed irradiation model simplifies the context with the assumption that all days of the year are sunny. Even on sunny days, there is some diffuse radiation, mainly due to the refusal of direct radiation by the molecules of the air. The total solar radiation is a sum of the direct, the diffuse and the ground reflected component of radiation. In this model the ground reflected component is insignificant because the location of the solar power plant is assumed to be in isolated rural areas [14-21].

The proposed PV grid inter-shading model is checked against commercial CAD software for visualization – PV Sol and ARCHICAD. Randomly chosen moments of date and time are evaluated and visualized in the CAD, and they all perfectly match the corresponding model's configuration and case. By implementing the model of inter-shading and using equa-

tions from eqs. (32)-(40) the power output can be calculated for a moment in a day, as well as monthly and yearly nominal energy. Figure 11 shows the daily power output for 4 days in a year (one day per season).

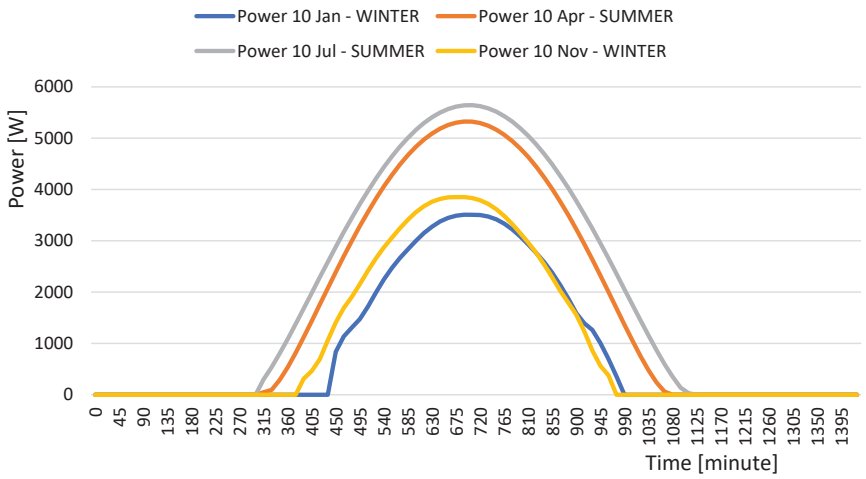

Figure 11. Daily power output

A useful application of the PV grid inter-shading model can be assessing the optimal density of a PV grid in populating available surface at a certain latitude while keeping the inter-shading insignificant as loss. An example analysis is given with the following parameters:

– geolocation: Skopje, Macedonia: latitude = 42˚ and longitude = 21.43˚
– grid geometry: $P_x = 0.81$ m, $P_y = 1.60$ m, $r_x = 0.5$ m ~ 5 m, $r_y = 0.5$ m ~ 5 m, panel azimuth $az = 0$˚, tilt angle $\beta = 32$˚
– grid occupied surface: $(3P_x + 2r_x) \times (3P_y\cos\beta + 2r_y)$

Table 1 shows annual energies and corresponding energy densities for combinations of distances between photovoltaic panels r_x and r_y in range from 0.5 m to 5 m. Calculations are made for optimal angle of inclination (tilt angle $\beta = 32$˚). Some investigators have made different recommendations for the optimum tilt angle, based on the latitude Kalogirou [21] suggests the optimum tilt angle to be latitude ± 10˚. The annual productions for the tilt angles of 32˚, 42˚ and 52˚ were analyzed and according to the obtained data 320 was determined as yearly optimal tilt angle for the region of Skopje, Macedonia.

Table 1. Energy [MWh]/Energy density [MWhm^{-2}]

	$r_x = 0.5$ m	$r_x = 1.0$ m	$r_x = 1.5$ m	$r_x = 5$ m
$r_y = 0.5$ m	12.94 0.74	13.02 0.58	12.81 0.47	13.05 0.21
$r_y = 1.0$ m	13.03 0.63	13.08 0.49	13.06 0.40	13.14 0.17
$r_y = 1.5$ m	13.07 0.54	13.10 0.42	13.07 0.34	13.17 0.15
$r_y = 5$ m	13.09 0.27	13.09 0.21	13.04 0.17	13.10 0.07

Obviously, the shorter the distances between panels the greater the inter-shading resulting in lower energy production. If panels are set at greater distances (1.5 m or 5 m) there is

no inter-shading between them, and larger energy is output but at cost of the larger area. At the distances of r_x = 0.5 m and r_y = 0.5 m the highest energy density is obtained, reduced annual output compared to distances r_x = 5 m and r_y = 5 m, but with 10 times more efficiently used surface area. The analysis allows estimating how much inter-shading can be tolerated against increasing the number of installed photovoltaic panels on the same surface.

Conclusion

This paper proposes a model for panel inter-shading estimation within a PV grid. It considers as input parameters the panel and grid geometry, its geolocation and a moment within the year (particular date and time in a day). The model is verified with a comparative analysis with commercial software packages visually confirming the azimuth-based situations. It is also validated through the power calculations resulting in analytically and statistically logical values under seasonal, daily and latitudinal circumstances. Analytics based on this model provides results that are a good basis for further techno-economic analysis aiding in the development of a methodology for optimal PV grid design for a given surface. The goal of the optimization is to maximize energy production in a minimal area with acceptable losses.

References

[1] Wang, Q., *et al.*, Dynamic Modeling and Small Signal Stability Analysis of Distributed Photovoltaic Grid-Connected System with Large Scale of Panel Level DC Optimizers, *Applied Energy, 259* (2020), Feb., pp. 114132
[2] Kassai, M., Experimental Investigation of Carbon Dioxide Cross-Contamination in Sorption Energy Recovery Wheel in Ventilation System, *Building Services Engineering Research & Technology, 39* (2018), 4, pp. 463-474
[3] Chatterjee, A., *et al.*, Design and Experimental Investigation of Digital Model Predictive Current Controller for Single Phase Grid Integrated Photovoltaic Systems, *Renewable Energy*, *108* (2017), Aug., pp. 438-448
[4] Kassai, M., Simonson, C. J., Experimental Effectiveness Investigation of Liquid-To-Air Membrane Energy Exchangers under Low Heat Capacity Rates Conditions, *Experimental Heat Transfer, 29* (2016), 4, pp. 445-455
[5] Soteris, A., *Solar Energy Engineering Process and Systems*, Elsevier, Amsterdam, The Netherlands, 2009
[6] Xiao, W., *et al.,* Topology Study of Photovoltaic Interface for Maximum Power Point Tracking, *IEEE Transactions on Industrial Electronics, 54* (2007), 3, pp. 1696-1704
[7] Patel, H., Agarwal, V., MATLAB-Based Modeling to Study the Effects of Partial Shading on PV Array Characteristics, *IEEE Transactions on Energy Conversion, 23* (2008), 1, pp. 302-310
[8] Duffie, J. A., Beckman, W. A., *Solar Engineering of Thermal Processes*, 4 ed., John Wiley and Sons, New York, USA, 2013
[9] Demsar, T., Optimisation of Quantity of Electric Energy from Solar Power Plant Regarding Its Layout (in Slovenian), M.Sc. thesis, University of Ljubljana, Ljubljana, 2016
[10] Stanciu, C., Stanciu, D., Optimum Tilt Angle aor Flat Plate Collectors All over the World–A Declination Dependence Formula and Comparisons for Three Solar Radiation Models, *Energy Conversion and Management,* Elsevier, Amsterdam, The Netherlands, Vol. 81, pp. 133-143, 2014
[11] Yadav, A. K., Chandel, S. S., Tilt Angle Optimization to Maximize Incident Solar Radiation: A Review, *Renewable and Sustainable Energy Reviews*, Elsevier, Amsterdam, The Netherlands, Vol. 23(C), pp. 503-513, 2013
[12] Stanciu, D., *et al.,* Mathematical Links between Optimum Solar Collector Tiltsin Isotropic Sky for Intercepting Maximum Solar Irradiance, *Journal of Atmospheric and Solar – Terrestrial Physics*, Elsevier, Amsterdam, The Netherlands, Vol. 137, pp. 58-65, 2015
[13] Li, H., *et al.,* Calculating the Diffuse Solar Radiation in Regions without Solar Radiation Measurements, *Energy*, *44*, (2011) 1, pp. 611-615
[14] Yadav, A. K., Chandel, S. S., Tilt Angle Optimization to Maximize Incident Solar Radiation: A Review, *Renewable and Sustainable Energy Reviews*, Elsevier, Amsterdam, The Netherlands, Vol. 23, 2013

[15] ***, Royal Greenwich Observatory, Science and Engineering Research Council, "Information Leaflet No.13: "The Equation of Time", http://www.oarval.org/equation.htm
[16] Mitkovic, M. P., *et al.,* Analysis of Electric Power Production in South Serbia: Recommendations for Improvement of Operation of First Mini Photovoltaic Power Plants, *Thermal Science*, *22* (2018), Suppl. 4, pp. S1205-S1216
[17] Milosavljević, D. D., *et al.*, Energy Efficiency of Photovoltaic Solar Plant in Real Climate Conditions in Banja Luka, *Thermal Science*, *19* (2015), 2, pp. 331-338
[18] Pavlovic, T. M., *et al.,* Simulation of Photovoltaic Systems Electricity Generation Using Homer Software in Specific Locations in Serbia, *Thermal Science*, *17* (2013), 2, pp. 333-347
[19] Spasevska, H., Solar Energy in Macedonia: Policy, Perspectives and Challenges for Application, *Proceedings,* World Renewable Energy Congress – XI, Abu Dhabi, UAE, pp. 1409-1414, 2010
[20] Kirn, B., *et al.,* Effective Load Carrying Capability of Solar Photovoltaic Power Plants – Case Study for Slovenia, Safety & Reliability: Theory and Applications, *Proceedings,* 27th European Safety and Reliability Conference, ESREL 2017, Portorož, Slovenia, 18-22 June 2017. Boca Raton: CRC Press; London: Taylor & Francis, 2017, Pages 3231-3239
[21] Kalogirou, S. A., The Potential of Solar Industrial Process Heat Applications, *Appl. Energy, 76* (2003), 4, pp. 337-361

Paper submitted: January 16, 2020
Paper revised: April 11, 2020
Paper accepted: April 21, 2020